Dalton Transactions

Accepted Manuscript

This article can be cited before page numbers have been issued, to do this please use: Y. Li and P. A. Korzhavyi, *Dalton Trans.*, 2016, DOI: 10.1039/C6DT04376C.

ROYAL SOCIETY OF CHEMISTRY

rsc.li/dalton

Journal Name

ARTICLE TYPE

Cite this: DOI: 10.1039/xxxxxxxxxx

Physical and chemical properties of Cu(I) compounds with O and/or H

Yunguo Li,*[a‡] and Pavel A. Korzhavyi,*[a]

Received Date
Accepted Date

DOI: 10.1039/xxxxxxxxxx

www.rsc.org/journalname

The electronic structure and chemical bonding of the Cu(I) compounds with O and/or H are investigated using *ab-initio* calculations based on density functional theory. A hybrid functional PBE0 is employed, which accurately reproduces the experimental band gap of cuprite Cu_2O. Cuprous hydroxide CuOH (cuprice) is found to be an indirect band gap semiconductor. Depending on the bond network configuration of CuOH, its band gap is found to vary between 2.73 eV and 3.03 eV. The presence of hydrogen in CuOH has little effect on the character of Cu–O bonds, as compared to Cu_2O, but lowers the energy levels of the occupied states upon the O–H bond formation. The bonding charge density and electron localization function calculations reveal that a closed-shell Cu–Cu interaction takes place in Cu_2O and CuOH between the neighbouring Cu cations belonging to different bond networks. Besides, three structures of cuprous hydride CuH are investigated. We find that the halite structure of CuH can be stabilized at high pressure (above 32 GPa) while the wurtzite is the most stable structure of CuH at ambient pressure. The H–H interaction contributes to the dynamical stabilization of the halite structure. The wurtzite and sphalerite structures of CuH are predicted to be semiconducting with small band gaps, while the halite structure is calculated to be metallic.

1 Introduction

Copper is recognized as one of the most important metals and has diverse applications[1–5]. Copper compounds containing oxygen and hydrogen are strongly relevant to the applications where copper metal is exposed to oxygen and water[1–5]. For some applications, where the system is driven out of equilibrium, the knowledge of the structure and properties of stable as well as metastable compounds is necessary for for understanding, predicting, and controlling the behavior of copper. Although Cu_2O and CuOH have been detected as products of copper corrosion under anoxic conditions[4,6–8], some circumstances of such corrosion behavior are still unclear[9,10].

The monovalent copper (cuprous) compounds with oxygen and hydrogen are generally less stable (and less studied) than their divalent counterparts[11,12]. Among the Cu(I) compounds, cuprous oxide Cu_2O (cuprite) is the only stable and the best studied one[13]. The crystal structure of Cu_2O may be viewed as a superposition of two identical anti-cristobalite lattices: two identical, interpenetrating (but disconnected) bond networks are obtained if one connects each Cu cation with the two nearest-neighbor O anions in the cuprite structure. A crystalline form of cuprous hydroxide CuOH was recently investigated theoretically and experimentally[11,12]. Its atomic structure is found to resemble that of Cu_2O, but with half of the Cu^+ ions substituted by protons. In contrast to the cuprous ions, which keep the central position in between the two nearest O^{2-} ions, the protons in CuOH form a shorter chemical bond with one of the two neighboring anions, while staying connected with the other anion via a hydrogen bond. The proton's freedom to chemically bind to either of the two anions in CuOH results in the so-called proton disorder that is typical of many hydroxides and phases of ice. Also, it was found that collective electrostatic interaction stabilizes a cation-ordered ground-state structure of CuOH[14].

Copper hydrides are not stable at atmospheric hydrogen pressure in the Cu–H system[15], but as metastable compounds they may be relevant to the applications of copper in which hydrogen entry into the metal is expected. Accumulation of hydrogen at defects in copper metal is known to cause formation of gas-filled voids acting as sources of stress in the material[16–18]. The formation of local hydride-like atomic configurations at lattice defects has been discussed in the context of void nucleation[19] and as a possible mechanism of hydrogen-induced embrittlement of metals[20]. Cuprous hydride was first reported by Wurtz[21] in 1884. Its crystal structure was studied using X-ray diffraction in 1926 by

[a] *Division of Materials Technology, Department of Materials Science and Engineering, Royal Institute of Technology (KTH), S-100 44 Stockholm, Sweden; E-mail: yunguo@kth.se; pavelk@kth.se*

‡ Present address: Crystallography and Mineral Physics, Department of Earth Sciences, University College London, Gower Street, London WC1E 6BT, United Kingdom.

two groups, Hüttig and Brodkorb[22] and Müller and Bradley[23], who reported, respectively, a cubic and a hexagonal lattice of copper ions. The structure was solved using neutron diffraction by Goedkoop and Andresen[24] in 1955 to be the hexagonal wurtzite structure, and further refined in several recent studies taking into account the non-stoichiometry of CuH_{1-x}[25–27].

Besides, a high-pressure phase of CuH with a face-centered cubic (fcc) arrangement of the copper atoms has been reported[28]. There are two possibilities for hydrogen in an fcc CuH structure, namely, to occupy tetrahedral interstitial positions (as in the sphalerite ZnS type structure) or to occupy the octahedral positions (as in the halite NaCl type structure). The sphalerite and wurtzite structures have been shown to be quite close in energy[11,29], while at a compressed volume approaching that of fcc Cu, hydrogen atoms tend to occupy octahedral interstital sites as in dilute Cu–H solid solutions[18,30]. The thermodynamic information about the halite phase of CuH is therefore of relevance for thermodynamic Calphad-type modeling of the solid solution of hydrogen in copper metal[31].

While the non-stoichiometry, disorder, and instability of the Cu(I) compounds with O and/or H represent challenges for experimental studies, in computer simulations the non-stoichiometry and disorder can be effectively excluded or included in order to investigate their effect on the properties. Here we use *ab initio* electronic structure calculations and a hybrid functional approach to explore the structures and properties of the cuprous oxide, hydroxide and hydride, to deepen our understanding of these compounds.

2 Methodology

2.1 Total energy calculation

All our calculations were performed using the Vienna *ab initio* simulation package (VASP) based on the density functional theory (DFT),[32,33] applying the projector augmented wave (PAW) potentials.[34–36] The Cu-$3d^{10}4s^1$, O-$2s^22p^4$, and H-$1s^1$ electron states were treated as valence. The exchange-correlation effects were included by means of the Perdew, Burke and Ernzerhof (PBE) functional[37] and the hybrid PBE0 functional[38]. The latter combines 25% of the non-local Hatree-Fock (HF) exchange with 75% of the PBE exchange, while keeping 100% of the PBE correlation energy. A plane-wave cut-off energy of 800 eV was tested to be enough to reach convergence.

The k-mesh was centered at the Γ-point; the separation between the k-points was approximately 0.03 $Å^{-1}$. The relaxation of the electronic degrees of freedom was stopped when the energy convergence was within 10^{-6} eV. The atomic relaxation was stopped when the force on each atom was less than 10^{-4} eV/Å. In what follows, we report the results of PBE and PBE0 calculations that have been performed, respectively at the PBE and PBE0 lattice parameters, unless otherwise stated.

2.2 Phonon spectrum calculations

A supercell approach was used to calculate the elements of the Hessian matrix based on density functional perturbation theory (DFPT) and PBE functional implemented in VASP. Then the phonon spectrum was derived by means of the PHONOPY code,[39] which is an implementation of post-process phonon analyzer. The phonon-related thermal properties of these compounds were then derived from the calculated phonon spectra in the quasi-harmonic approximation. The vibrational energy $E_{\mathrm{vib}}(V,T)$ and the vibrational entropy S_{vib} were thus obtained. The Helmholtz free energies $F(V,T)$ are expressed for the considered compounds by

$$F(V,T) = E_{\mathrm{el}}(V,0) + E_{\mathrm{vib}}(V,T) - T \cdot S_{\mathrm{vib}} \quad (1)$$

where $E_{\mathrm{el}}(V,0)$ is the ground-state total electronic energy calculated using VASP within the DFT framework using the PBE (or PBE0) functional.

2.3 Differential charge density and electron localization function

Conventionally, the differential charge density is calculated by subtracting from the charge density of a crystal the superimposed charge densities of ions or atoms. Since both the cuprous oxide and the hydroxide are constructed by interpenetrating two identical bond networks (hereafter also referred to as "lattices"), we calculated the differential charge density by subtracting from the charge density of the crystal the superimposed charge densities of the two lattices calculated separately (keeping fixed the supercell geometry and the atomic positions). In this way, information about the interaction between the lattices can be obtained. The so defined differential charge density is given by

$$\rho_D = \rho_{\mathrm{crystal}} - (\rho_{\mathrm{lattice1}} + \rho_{\mathrm{lattice2}}) \quad (2)$$

The electron localization function (ELF)[40,41] is a measure of the electron localization in real space and helps to characterize the chemical bonding. ELF is expressed in terms of the ratio between the excess of kinetic energy density due to the Pauli exclusion principle, $t_p(r)$, to the Thomas-Fermi kinetic energy density $t_h(\rho) = (3/10)(3\pi)^{2/3}\rho^{5/3}$ of a homogeneous electron gas of density ρ. Within the Kohn-Sham scheme, the increase in kinetic energy that occurs on consideration of Pauli principle is evaluated as

$$t_p(r) = \frac{1}{2}\sum_i |\nabla\varphi_i|^2 - \frac{1}{8}\frac{|\nabla\rho(r)|^2}{\rho(r)} \quad (3)$$

where the first term is the kinetic energy obtained from Kohn-Sham orbitals φ_i and the second term gives the kinetic energy density for the same density distribution $\rho(r)$ when the Pauli principle is ignored.

The ELF can then be evaluated at any point r as follows:

$$\mathrm{ELF} = \left\{1 + \left[\frac{t_p(r)}{t_h(\rho(r))}\right]^2\right\}^{-1}. \quad (4)$$

The ELF has values in the range between 0 and 1, with the upper limit corresponding to the highest degree of localization of the electrons.

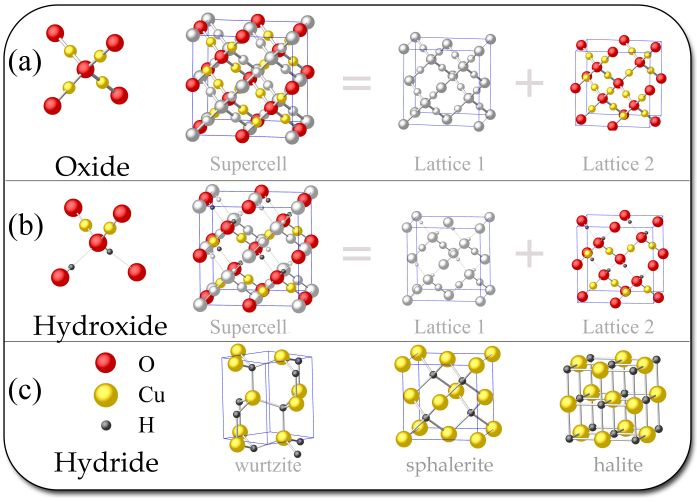

Fig. 1 Ball-and-stick representation of the crystal structures: (a) cuprous oxide (cuprite), panels from left to right show, respectively, coordination of oxygen in Cu_2O, supercell obtained by 2×2×2 repetition of the unit cell, and two identical anti-cristobalite Cu_2O lattices; (b) cuprous hydroxide (cuprice), panels from left to right show, respectively, coordination of oxygen in CuOH, supercell containing 16 CuOH units, and two identical CuOH lattices; (c) three considered structures of cuprous hydride, respectively, a hexagonal (wurtzite) and a cubic (sphalerite) CuH with hydrogen in tetrahedral positions, and a cubic (halite) CuH with hydrogen in octahedral positions.

3 Results and Discussion

3.1 Crystal structures

Cu_2O possesses the cuprite crystal structure (space group $Pn\bar{3}m$), which can be viewed as consisting of two interpenetrating anti-cristobalite lattices depicted in Figure 1(a). The O^{2-} anion sublattice is body-centered cubic (BCC) and splits into two diamond structures when the ionic coordination is considered: Each O^{2-} anion is tetrahedrally coordinated by four Cu^+ cations, while each Cu^+ cation is linearly coordinated by two anions (7). All the Cu^+ ions taken together constitute a face-centered cubic (FCC) cation sublattice in Cu_2O.

The molecular form of cuprous hydroxide CuOH has been been known for some time.[42,43] However, the structure of a condensed form of CuOH was only recently investigated by Korzhavyi *et al.* in a combined theoretical and experimental study.[11,12] The proposed crystalline form of CuOH was given the name "cuprice", to address its structural resemblance to both cuprite and ice. The structure of cuprice is intermediate between the crystal structures of cuprite and ice VII (the latter is also comprised of two interpenetrating cubic ice I_c lattices). Thus, the O^{2-} anions in cuprice CuOH may be viewed as arranged into the same BCC sublattice (or two interpenetrating diamond sublattices) as in cuprite Cu_2O. The cuprous cations and protons in CuOH are coordinated in the same way as in Cu_2O (cuprite) and ice H_2O (cubic ice I_c), respectively.[11] These coordination rules allow for many different configurations of protons and cuprous cations, in which each oxygen should be tetrahedrally coordinated by two cuprous cations and two protons to maintain the CuOH stoichiometry. One proton is to be located closer to the central oxygen position and the second proton is to be located further away from the anion (thus forming a hydrogen bond). The smallest unit cell of such kind (denoted by its space group $Cm2a$ in Table 1) contains two CuOH molecular units (two O^{2-}, two H^+, and two Cu^+ ions). A CuOH supercell that corresponds to the 2×2×2 supercell of Cu_2O and contains 16 CuOH formula units is shown in Figure 1(b). We have explored different possible distributions of protons and cuprous ions in the CuOH supercell, compatible with the local coordination rules discussed above, to find that they form different CuOH supramolecular units having different multipole charges. Their collective electrostatic interaction selects the ground-state structure (cation-ordered, antiferroelectric) of cuprice.[14]

Table 1 Lattice parameters and band gaps of Cu_2O, CuOH, and CuH calculated using PBE and PBE0 functionals.

Formula	Space group	Lattice parameters (Å)		Band gap (eV)	
		PBE	PBE0	PBE	PBE0
Cu_2O	$Pn\bar{3}m$	a = 4.31	a = 4.30	0.48	2.17
CuOH	$Cm2a$	a = 5.70 b = 5.30 c = 4.21	a = 5.73 b = 5.33 c = 4.14	0.80	2.73
CuH	$P6_3mc$	a = 2.89 c = 4.57	a = 2.87 c = 4.58	0.53	1.26
	$F\bar{4}3m$	a = 4.02	a = 4.02	0.54	1.48
	$Fm\bar{3}m$	a = 3.90	a = 3.90	0	0

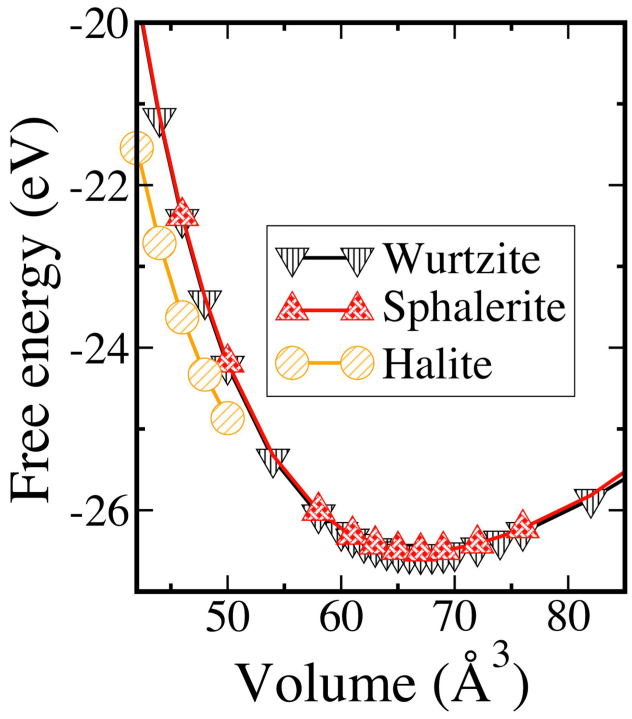

Fig. 2 Calculated Helmholtz free energies F(V, 0) of the three CuH structures.

The crystal structure of copper hydride observed in experiments[28,44] is the hexagonal CuH (wurtzite, space group $P6_3mc$), as shown in Figure 1(c). The sphalerite CuH structure (space group $F\bar{4}3m$) with hydrogen in tetrahedral positions is reported

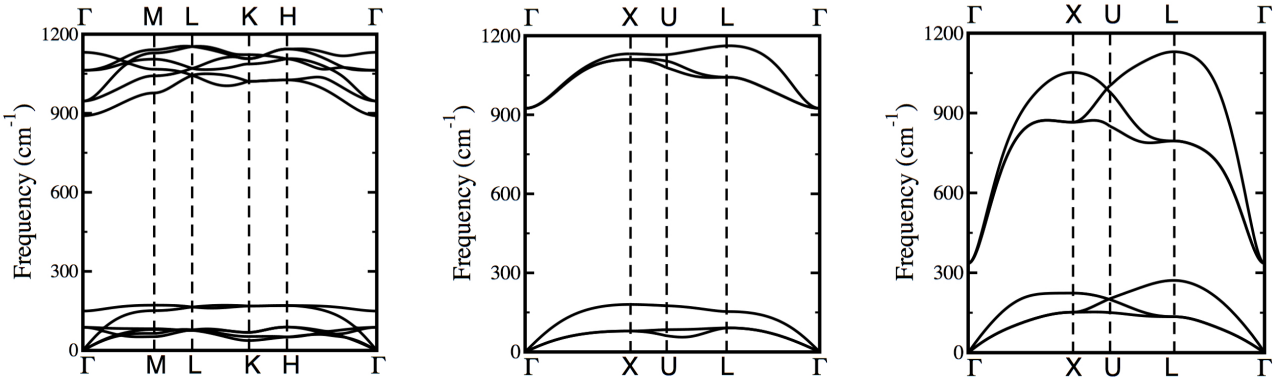

(a) wurtzite (b) sphalerite (c) halite

Fig. 3 Calculated phonon spectra of CuH in three different crystal structures. The halite structure is considered at a reduced unit cell volume of 50 Å^3. The wurtzite and sphalerite structures are at their equilibrium volumes.

to be slightly less stable[29] than the hexagonal structure and is less frequently observed in experiments. The free energies from our calculations are shown in Figure 2. Both the wurtzite and the sphalerite structures are dynamically stable in the examined pressure range. The halite (space group $Fm\bar{3}m$) with hydrogen in octahedral interstitial positions corresponds to the structure of FCC-copper with all octahedral sites filled with hydrogen. This structure is dynamically unstable when the pressure is below 32 GPa (the volume of unit cell less than 50 Å^3). From 32 GPa and above, it is dynamically stable. The stabilization will be shown below to be attributed to the enhanced strength of H-H bonding. As can be seen in Figure 3(c), the optic hydrogen modes disperse over 800 cm^{-1} and the lower frequency reaches to 336 cm^{-1}. Below 32 GPa, the optic hydrogen modes show imaginary frequencies. This also indicates the stabilization of H-H bonding. At high pressure (higher than 32 GPa), the halite CuH becomes the most stable of the examined hydride structures. The corresponding phonon spectra are shown in Figure 3. Table 1 shows the crystallographic data for the studied structures of Cu(I) oxide, hydroxide, and hydride.

3.2 Density of states

The PBE0-calculated band gap values are given in Table 1; the electronic densities of states (DOS) are shown in Figure 4. Cu_2O is the only semiconductor with a direct band gap among the studied Cu(I) compounds. Figure 4(a) shows the DOS of Cu_2O with a clear gap between the Cu-3d and O-2p states. The PBE0-calculated band gap of cuprous oxide, $E_g = 2.17$ eV, is in good agreement with the experimental data (2.0−2.2 eV).[45,46] The upper valence band is dominated by Cu-3d states, with two main groups of peaks centered at about −1.0 eV and −2.5 eV. The O-2p dominated states are situated at lower energies, bound by two peaks at −6.5 eV and −7.5 eV. A sharp peak of O-2s states is situated at −21.3 eV.

The atomic structure of CuOH resembles that of Cu_2O but with half of the Cu^+ replaced by protons.[11] The two protons bound to each O^{2-} lay at different distances from the O^{2-} anion: one is closer (0.973 Å) while the other is further away (2.204 Å). It is therefore interesting to investigate how the electronic structures of CuOH and Cu_2O are related. Figure 4(b) shows the DOS of CuOH $Cm2a$ structure. The valence O-2p states are split into two groups of peaks centered, respectively, at about −6.5 and −9.0 eV. The peak at −6.5 eV is contributed by states of p_x, p_y and p_z character, while the other peak by p_x and p_y states. The O−H bonding can be speculated to be a result of hybridization between the H-1s and O-2p states, to produce bonding and antibonding peaks. The antibonding peaks at around −6.5 eV contain some admixture from Cu states. The charge transfer between the ionic species in cuprous oxide and hydroxide is represented by the computed Bader charges in Table 2: the copper cation is found to donate more charge to the oxygen anion in the hydroxide. The hybridization with the H-1s states is calculated to lower the occupied states and to widen the band gap. As can be seen from Table 1, the band gap of CuOH is larger than that of Cu_2O. The positioning of protons and copper cations in CuOH allows for many different configurations, which should be of similar energy as all these structural variants have identical number of chemical bonds. However, collective electrostatic interactions in CuOH can be so prominent that the energy span between the ground-state structure and the least-stable structure is 7.49 kJ/mol CuOH.[14] Cation ordering, via the collective electrostatic interactions, also influences the electronic spectrum. Thus, the the band gap of CuOH is calculated to vary from 2.73 eV (the least stable structure) to 3.03 eV (the ground-state structure). The mechanism of this influence is re-distribution of electron charge between the ionic species as a result of electrostatic interaction: The occupancy of the Cu-4s state in the ground-state structure (0.203) is reduced compared to the least-stable structure (0.210). As the occupancy of Cu-4s state is reduced, the excess charge is transferred to the O−H antibonding state, whose energy level is lowered, so the band gap slightly opens up.

The two structures of CuH with hydrogen in tetrahedral positions, the wurtzite and the sphalerite, are semiconductors. Their calculated band gaps are summarized in Table 1, and the DOS are shown in Figure 4(c) and (d). As can be seen from the Figure, Cu-4s and H-1s states are strongly mixed. The main peaks of

Table 2 Computed Bader charges (in |e|) for Cu_2O, CuOH, and CuH using PBE and PBE0 functionals.

Material	Bader Charge (|e|)					
	PBE			PBE0		
	Cu	O	H	Cu	O	H
Cu_2O	+0.538	−1.075	–	+0.566	−1.133	–
CuOH	+0.549	−1.175	+0.374	+0.577	−1.232	+0.345
CuH (wurtzite)	−0.339	–	+0.339	−0.326	–	+0.326
CuH (sphalerite)	−0.385	–	+0.385	+0.374	–	−0.374
CuH (halite)	−0.238	–	+0.238	+0.231	–	−0.231

the d-band lie between −2.9 eV and −5.9 eV for the wurtzite and the sphalerite. Two more weak peaks of d character appear at higher energies, with certain admixture of Cu-4s and H-1s states. This is probably due to the d-band self-depletion as a result of s-d hybridization. The other considered structure (halite) of CuH, with hydrogen in octahedral positions, is calculated to be a metal; its band structure (with some bands crossing the Fermi level) is shown as the inset of Figure 4(e). The electronic structure of CuH(halite) shown in Figure 4(e) corresponds to a compressed unit cell volume of 50 Å^3. All the occupied states shift downwards relative to the Fermi level when pressure is applied. The Bader charge on the copper ions in the halite CuH is the lowest among the studied hydride structures (see Table 2), whereas the corresponding Cu–H bond length is the largest.

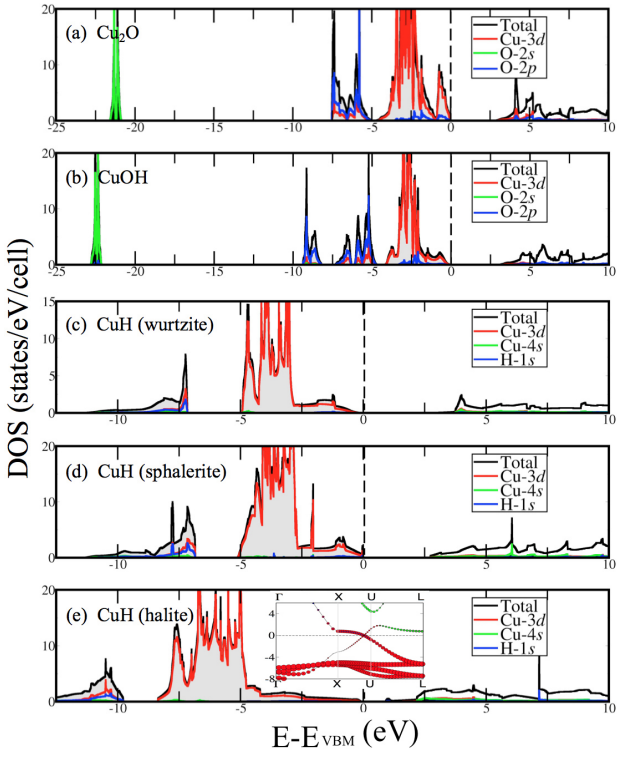

Fig. 4 (a-e): PBE0-calculated DOS for cuprite Cu_2O, cuprice CuOH, and three structures of CuH. The element-specific DOS are projected from the Kohn-Sham wave functions onto the Bader atomic volumes. The inset in (e) is the PBE0-calculated band structure of halite CuH. All energies are relative to the valence band maximum (VBM).

Synthesized CuH usually suffers from non-stoichiometry: the hydrogen positions in the wurtzite structure are not fully occupied. To study the effect of hydrogen vacancies in substoichiometric CuH_{1-x} on its electronic structure we performed supercell calculations in which the wurtzite unit cell was duplicated along the $\vec{a}$, $\vec{b}$, and $\vec{c}$ directions and one hydrogen atom was removed from the so obtained supercell. As can be seen in Figure 5, with 1/16 of hydrogen positions being vacant, the Fermi level is shifted into the valence band, which leads to the metallicity and suggests the p-type doping nature of a hydrogen vacancy defect. The hydride should remain semiconducting with less amount of vacancy, while the bandgap must always be lower than its ideal value. The non-stoichiometry problem also exists in the case of cuprice CuOH. Its structure may incorporate a large amount of intrinsic configurational disorder which we have studied in a previous publication.[14] In addition, experimental CuOH specimens typically contain extrinsic defects such as inclusions of H_2O, Cu_2O, and CuO. The physical and chemical properties of the synthesized CuOH may be expected to show the behaviour of phase mixtures.[12]

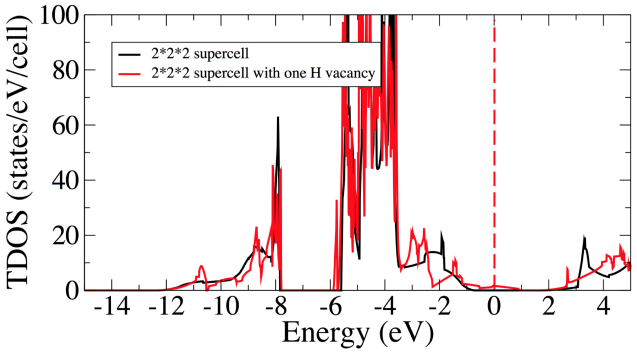

Fig. 5 PBE0-calculated DOS for the wurtzite CuH with H vacancy (one H vacancy in a 2×2×2 supercell).

3.3 Chemical bonding

The band gaps in the electronic spectra of Cu_2O cuprite, CuOH cuprice, CuH wurtzite, and CuH sphalerite indicates that the chemical bonding in these Cu(I) compounds is of mixed ionic-covalent character. Their crystal structures exhibit local coordination typical of compound semiconductors, and this structural aspect suggests that the covalent component of bonding is prevalent. On the other hand, the calculated Bader charges listed in Table 2 and ELF plots shown in Figure 6 indicate that the ionic

component of chemical in the studied Cu(I) compounds is rather strong. For cuprous oxide, this picture of chemical bonding agrees with the findings made in the previous theoretical studies.[47–53]

The ELF of Cu_2O is shown in Figure 6 (a); the scale is encoded using a color scheme in which values corresponding to a high degree of electron localization are shown in red while regions of low ELF values are shown in blue. At the Cu cation sites the ELF takes on low values, whereas spherical regions of high ELF (0.85) can be seen around the sites of O anions. Such large difference in the ELF is a signature of the strong ionic character of Cu–O bonding. Besides, there is a weak doughnut-shaped halo of ELF around each Cu^+ cation in Cu_2O, with the symmetry axis parallel (and the mirror plane perpendicular) to the O–Cu–O bond network segment.

The ELF of cuprice CuOH shown in Figure 6(b) suggests a covalent character of bonding between O and the closest H, which jointly form a hydroxyl OH^- group by sharing an electron, while the Cu sites are still characterized by low values of ELF. There is no lobe protruding from a Cu site towards the nearest O sites, suggesting that the Cu–O bond is still ionic in CuOH. Besides, the weak halo of ELF around Cu^+ as in Cu_2O is also found in CuOH. Such feature has been attributed to 3*d*-shell depletion and *s*-*d* hybridization of Cu^+, which leads to a weak interaction between Cu cations that stabilizes the cuprite structure of Cu_2O.[47–49,53]

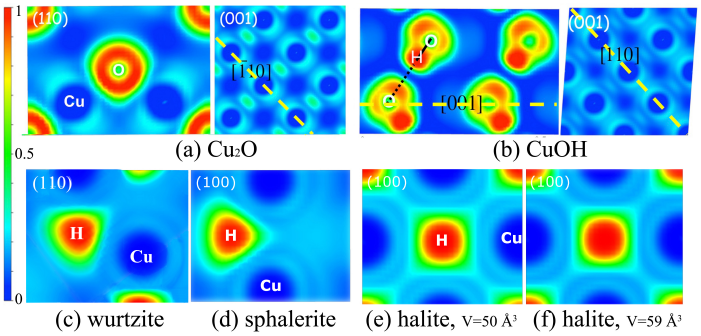

Fig. 6 ELF contour plots of (a) the cuprite Cu_2O, (b) the cuprice CuOH and (c-f) the three CuH structures.

Shown in Figure 7 are the differential charge densities of cuprite Cu_2O and cuprice CuOH. In both compounds, the major charge redistribution due to the interaction between the two disconnected bond networks (lattices) occurs around the Cu cations. In the oxide, the charge depletes from the Cu–O bond and accumulates in the doughnut around the Cu cation oriented perpendicular to Cu–O bond. In the hydroxide, the charge redistribution is more complex. For the supercell obtained by 2×2×2 repetition of the *Cm*2*a* unit cell, as well as for the least stable CuOH structure, the major charge depletion and accumulation take place in the (001) plane containing Cu cations. The regions of accumulated charge around Cu cations are dumbbell-shaped in these CuOH structures, at variance with the doughnut-shaped regions in Cu_2O. The difference is related to the Cu–Cu coordination: For each Cu cation in the oxide, there are six Cu nearest neighbours from the other lattice, all arranged into a hexagon belonging to a ⟨111⟩ plane. The number of such neighbors for each Cu cation in the hydroxide is two for the structure of 2×2×2 of the *Cm*2*a* unite cell and for the least stable structure, but either two or four for the ground-state structure. As seen in Figure 7(c), the shape of the accumulated charge around Cu cations of the ground-state structure is either more spherical (when the coordination number is four) or more dumbbell-like (when the coordination number is two). The calculated total amount of charge transfer (shown in the caption of Figure 7) is proportional to this coordination number. The larger the number, the stronger is the charge transfer. As our calculations show, there is still charge transfer caused by the inner lattice interaction even in the case of no Cu cations (e.g., in the antiferroelectric ice VIII), but its total amount is just 0.15e per cell. Apparently, Cu cations are more adaptable to such interaction as they generate substantial charge transfer.

Figures 6(c-f) show the ELF plots for the examined structures of CuH. For the wurtzite (Figure 6(c)) and sphalerite (Figure 6(d)) structures, the valence electrons strongly localize around H, and at the Cu sites the ELF has very low values. The shape of ELF clouds around H is not spherical, but tetrahedral, since the electrons feel repulsion from the closed shells of neighbouring Cu. Therefore, the Cu–H bonding in wurtzite and sphalerite CuH is of prevailingly ionic character. The shape of ELF around H in halite CuH (Figure 6(e) and (f)) is cubic as H is at the center of an octahedral site. The length of the Cu–H bond (1.95 Å at the unit cell volume of 59 $Å^3$) in the halite structure is much longer than that in the wurtzite and the sphalerite structures (1.74 Å), so the H ion is not well confined and the halite CuH is dynamically unstable until the bond length is decreased to 1.84 Å(by compressing the unit cell volume to 50 $Å^3$). Besides, there is an isthmus of ELF between neighbouring H as seen in Figure 6(e) and (f), and it becomes thicker when the halite structure is compressed. This ELF topology[54] suggests a shared-electron interaction between the hydrogens, and is compatible with the weak metallicity of halite CuH. It can be speculated that the H-H interaction also contributes to the stabilization of the halite structure at high pressure.

4 Conclusions

We have used *ab initio* calculations and a hybrid functional approach to explore the physical and chemical properties of the cuprous oxide, hydroxide and hydride. Several conclusions can be drawn from the above analyses:

(a) The PBE0 functional successfully reproduces the experimental band gap of cuprite Cu_2O. A closed-shell Cu–Cu interaction exists between the neighbouring Cu cations of different sublattices. This interaction is a result of charge correlations between the disconnected bond networks, and it depends on the mutual coordination of the Cu cations.

(b) Cuprous hydroxide CuOH is an indirect band gap semiconductor. The disorder of cations in CuOH can make its band gap vary between 2.73 eV and 3.03 eV. The hydrogen in CuOH has little effect on the ionic nature of the Cu–O bonding relative to that in Cu_2O, but lowers the energy levels of the occupied states by giving a covalent character to the O-H bond.

(c) The halite structure CuH is shown to be stable only at high pressure (above 32 GPa). The wurtzite and sphalerite structures

are more stable at low pressure, with the wurtzite being slightly lower in energy than the cubic polymorph. The wurtzite and sphalerite structures are semiconductors with small band gaps, while the halite structure is metallic. The H–H electron-sharing interaction contributes to the dynamical stabilization of the halite structure.

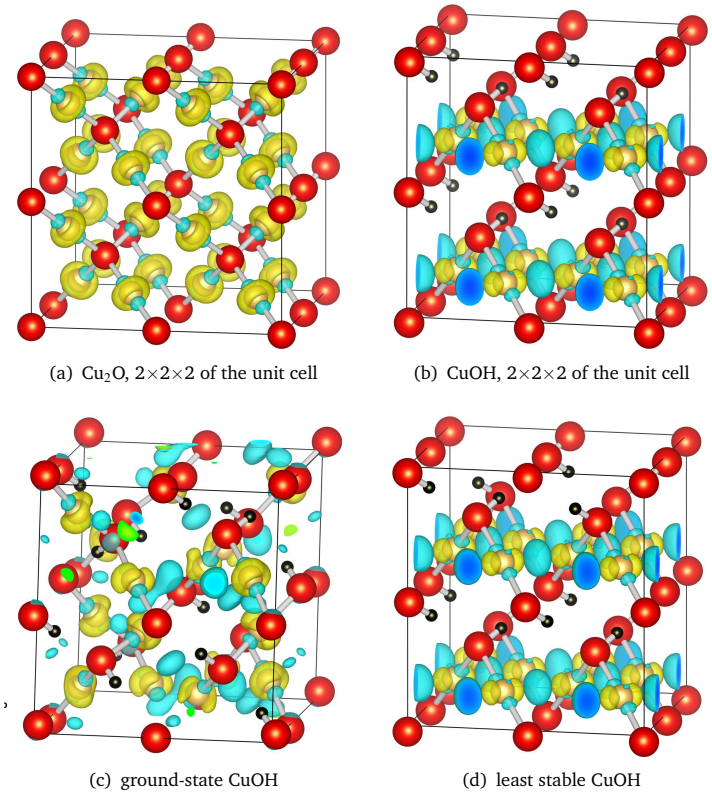

(a) Cu_2O, 2×2×2 of the unit cell (b) CuOH, 2×2×2 of the unit cell

(c) ground-state CuOH (d) least stable CuOH

Fig. 7 Differential charge density plots (yellow: charge accumulation, cyan: charge depletion): (a) cuprite Cu_2O, (b) 2×2×2 of the *Cm2a* unit cell of CuOH, (c) ground-state CuOH, and (d) least stable CuOH. The isosurface value is 0.003 eV/Å^3. The total charge transfer per cell for (a-d) are 1.74 e, 1.03 e, 1.12 e, and 1.02 e, respectively.

5 Acknowledgement

Financial support from the Swedish Nuclear Fuel and Waste Management Company (SKB) is gratefully acknowledged. Yunguo Li also thanks the Chinese Scholarship Council (CSC) for support. The computations were performed on resources provided by the Swedish National Infrastructure for Computing (SNIC) at the National Supercomputer Center (NSC), Linköping, the Abisko cluster at High Performance Computing Center North (HPC2N), Umeå, and at the PDC Center for High-performance Computing, Stockholm.

References

1 A. Atkinson, S. Barnett, R. J. Gorte, J. Irvine, A. J. McEvoy, M. Mogensen, S. C. Singhal and J. Vohs, *Nat. Mater.*, 2004, **3**, 17–27.

2 F. King and C. Padovani, *Corros. Eng., Sci. Technol.*, 2011, **46**, 82–90.

3 S. Jeong, H. C. Song, W. W. Lee, S. S. Lee, Y. Choi, W. Son, E. D. Kim, C. H. Paik, S. H. Oh and B.-H. Ryu, *Langmuir*, 2011, **27**, 3144–3149.

4 G. Hultquist, M. Graham, O. Kodra, S. Moisa, R. Liu, U. Bexell and J. Smialek, *Corrosion of copper in distilled water without molecular oxygen and the detection of produced hydrogen*, Swedish Radiation Safety Authority, SSM Technical Report 2013:07, SSM Report 2013:07, Swedish Radiation Safety Authority, 2013.

5 C. W. Li and M. W. Kanan, *J. Am. Chem. Soc.*, 2012, **134**, 7231–7234.

6 G. Hultquist, P. Szakalos, M. Graham, A. B. Belonoshko, G. Sproule, L. Gråsjö, P. Dorogokupets, B. Danilov, T. AAstrup and G. Wikmark, *Catal. Lett.*, 2009, **132**, 311–316.

7 G. Hultquist, M. Graham, P. Szakalos, G. Sproule, A. Rosengren and L. Gråsjö, *Corros. Sci.*, 2011, **53**, 310–319.

8 R. Becker and H.-P. Hermansson, *Evolution of hydrogen by copper in ultrapure water without dissolved oxygen*, Swedish Radiation Safety Authority, SSM Technical Report 2011:34, SSM Report 2011:34, Swedish Radiation Safety Authority, 2011.

9 M. Ottosson, M. Boman, P. Berastegui, Y. Andersson, M. Hahlin, M. Korvela and R. Berger, *Copper in ultra pure water*, Swedish Nuclear Fuel and Waste Management Company Technical Report TR-16-01, SKB Report TR-16-01, Swedish Nuclear Fuel and Waste Management Company, 2016.

10 C. M. Lousada, A. J. Johansson and P. A. Korzhavyi, *J. Phys. Chem. C*, 2015, **119**, 14102–14113.

11 P. A. Korzhavyi, I. L. Soroka, E. I. Isaev, C. Lilja and B. Johansson, *Proc. Natl. Acad. Sci. U.S.A.*, 2012, **109**, 686–689.

12 I. L. Soroka, A. Shchukarev, M. Jonsson, N. V. Tarakina and P. A. Korzhavyi, *Dalton Trans.*, 2013, **42**, 9585–9594.

13 P. A. Korzhavyi and B. Johansson, *Literature review on the properties of cuprous oxide Cu_2O and the process of copper oxidation*, Swedish Nuclear Fuel and Waste Management Company Technical Report TR-11-08, SKB Report TR-11-08, Swedish Nuclear Fuel and Waste Management Company, 2011.

14 Y. Li, C. M. Lousada, I. L. Soroka and P. A. Korzhavyi, *Inorg. Chem.*, 2015, **54**, 8969–8977.

15 T. B. Massalski, J. L. Murray, L. H. Bennett and H. Baker, *Binary alloy phase diagrams*, American Society for Metals Metals Park, OH, 1986, vol. 1.

16 W. R. Wampler, T. Schober and B. Lengeler, *Philos. Mag.*, 1976, **34**, 129–141.

17 Å. Martinsson, R. Sandström and C. Lilja, *Hydrogen in oxygen-free, phosphorus-doped copper: charging techniques, hydrogen contents and modelling of hydrogen diffusion and depth profile*, Swedish Nuclear Fuel and Waste Management Company Technical Report TR-13-09, SKB Report TR-13-09, Swedish Nuclear Fuel and Waste Management Company, 2013.

18 M. G. Ganchenkova, Y. N. Yagodzinskyy, V. A. Borodin and H. Hänninen, *Philos. Mag.*, 2014, **94**, 3522–3548.

19 J. B. Condon and T. Schober, *J. Nucl. Mater.*, 1993, **207**, 1–24.

20 G. P. M. Leyson, B. Grabowski and J. Neugebauer, *Acta Mater.*,

2015, **89**, 50–59.
21 A. Wurtz, *Cr. Hebd. Acad. Sci.*, 1844, **18**, 702–704.
22 G. F. Hüttig and F. Brodkorb, *Z. Anorg. Chem.*, 1926, **153**, 235–245.
23 H. Müller and A. J. Bradley, *J. Chem. Soc.*, 1926, **129**, 1669–1673.
24 J. A. Goedkoop and A. F. Andresen, *Acta Cryst.*, 1955, **8**, 118–119.
25 H. Auer and H. Kohlmann, *Z. Anorg. Allg. Chem.*, 2014, **640**, 3159–3165.
26 E. L. Bennett, T. Wilson, P. J. Murphy, K. Refson, A. C. Hannon, S. Imberti, S. K. Callear, G. A. Chass and S. F. Parker, *Acta Cryst. B*, 2015, **71**, 608–612.
27 E. Bennett, T. Wilson, P. J. Murphy, K. Refson, A. C. Hannon, S. Imberti, S. K. Callear, G. A. Chass and S. F. Parker, *Inorg. Chem.*, 2015, **54**, 2213–2220.
28 R. Burtovyy and M. Tkacz, *Solid State Commun.*, 2004, **131**, 169–173.
29 P. A. Korzhavyi and B. Johansson, *Thermodynamic properties of copper compounds with oxygen and hydrogen from first principles*, Swedish Nuclear Waste Management Company Technical Report TR-10-30, SKB Report TR-10-30, Swedish Nuclear Fuel and Waste Management Company, 2010.
30 P. A. Korzhavyi and R. Sandström, *Comput. Mater. Sci.*, 2014, **84**, 122–128.
31 H. Magnusson and K. Frisk, *Thermodynamic evaluation of Cu-HOSP system*, Swedish Nuclear Waste Management Company Technical Report TR-13-11, SKB Report TR-13-11, Swedish Nuclear Fuel and Waste Management Company, 2013.
32 G. Kresse and D. Joubert, *Phys. Rev. B*, 1999, **59**, 1758.
33 P. E. Blöchl, *Phys. Rev. B*, 1994, **50**, 17953.
34 G. Kresse and J. Furthmüller, *Comput. Mater. Sci.*, 1996, **6**, 15–50.
35 G. Kresse and J. Furthmüller, *Phys. Rev. B*, 1996, **54**, 11169.
36 G. Kresse and J. Hafner, *Phys. Rev. B*, 1993, **48**, 13115.
37 J. P. Perdew, K. Burke and M. Ernzerhof, *Phys. Rev. Lett.*, 1996, **77**, 3865–3868.
38 C. Adamo and V. Barone, *J. Chem. Phys.*, 1999, **110**, 6158–6170.
39 A. Togo, F. Oba and I. Tanaka, *Phys. Rev. B*, 2008, **78**, 134106.
40 A. Savin, O. Jepsen, J. Flad, O. K. Andersen, H. Preuss and H. G. von Schnering, *Angew. Chem. Int. Ed.*, 1992, **31**, 187–188.
41 A. D. Becke and K. E. Edgecombe, *J. Chem. Phys.*, 1990, **92**, 5397–5403.
42 M. Trkula and D. O. Harris, *J. Chem. Phys.*, 1983, **79**, 1138.
43 J. Kauffman, R. H. Hauge and J. Margrave, *J. Phys. Chem.*, 1985, **89**, 3541–3547.
44 R. Burtovyy, D. Włosewicz, A. Czopnik and M. Tkacz, *Thermochim. Acta*, 2003, **400**, 121–129.
45 M. Hara, T. Kondo, M. Komoda, S. Ikeda, J. N. Kondo, K. Domen, M. Hara, K. Shinohara and A. Tanaka, *Chem. Commun.*, 1998, 357–358.
46 S. N. Kale, S. B. Ogale, S. R. Shinde, M. Sahasrabuddhe, V. N. Kulkarni, R. L. Greene and T. Venkatesan, *Appl. Phys. Lett.*, 2003, **82**, 2100–2102.
47 J. Zuo, M. Kim, M. O'Keeffe and J. Spence, *Nature*, 1999, **401**, 49–52.
48 S.-G. Wang and W. E. Schwarz, *Angew. Chem. Int. Ed.*, 2000, **39**, 1757–1761.
49 J. Zuo, M. O'Keeffe, M. Kim and J. Spence, *Angew. Chem. Int. Ed.*, 2000, **39**, 3791–3794.
50 T. Lippmann and J. R. Schneider, *Acta Crystallogr., Sect. A: Found. Crystallogr.*, 2000, **56**, 575–584.
51 A. Buljan, M. Llunell, E. Ruiz and P. Alemany, *Chem. Mater.*, 2001, **13**, 338–344.
52 R. Laskowski, P. Blaha and K. Schwarz, *Phys. Rev. B*, 2003, **67**, 075102.
53 A. Filippetti and V. Fiorentini, *Phys. Rev. B*, 2005, **72**, 035128.
54 B. Silvi and A. Savin, *Nature*, 1994, **371**, 683–686.